ACS OMEGA

Open Access

http://pubs.acs.org/journal/acsodf

Article

Quercetin-Derived Platinum Nanomaterials Influence Particle Stability, Catalytic, and Antimicrobial Performance

Gaddi B. Eshun, Francis J. Osonga, and Omowunmi A. Sadik*

Cite This: *ACS Omega* 2024, 9, 38557−38568

Read Online

ACCESS | Metrics & More | Article Recommendations | Supporting Information

ABSTRACT: Quercetin possesses high biological properties but low bioavailability, poor solubility, and rapid body clearance. Its structural modification is imperative for enhanced applications. Herein, we demonstrate the catalytic and antimicrobial characteristics of shape-dependent (cuboidal and peanuts) platinum nanoparticles. Modified quercetin, 4′-QP, was employed as the reducing and stabilizing agent for the aqueous synthesis of PtNPs without extraneous reagents. Monodispersed platinum nanocubes (C-PtNPs) and nanopeanuts (P-PtNPs) were produced by reacting 4′-QP and Pt ions in the ratios of 3:1 and 1:1, respectively. TEM characterization confirmed the formation of Pt nanocubes and Pt nanopeanuts, with their corresponding sizes of 39.1 ± 0.20 and 45.1 ± 0.24 nm. The shape-dependency of PtNPs on the nosocomial-causing bacteria, *Citrobacter freundii* ATCC 8090 (*C. freundii*) was determined by the Agar well-diffusion assay. Under the same particle size and dose treatments, C-PtNPs and P-PtNPs exhibited 16.28 ± 0.10 and 4.50 ± 0.15 mm zones of inhibition with minimum inhibitory concentrations of 25 and 45 μg/mL, respectively. SEM analysis of C-PtNPs treated *C. freundii* showed a damaged cell membrane and confirmed contact-killing as the antibacterial mechanism. The catalytic conversion of 4-nitrophenol (4-NP) to 4-amino phenol (4-AP) was tested using a shape-dependent PtNPs catalyst in the presence of sodium borohydride. The conversion rates (k) of C-PtNPs and P-PtNPs in wastewater samples from New Jersey were 0.0108 and 0.00607 s^{-1}, respectively.

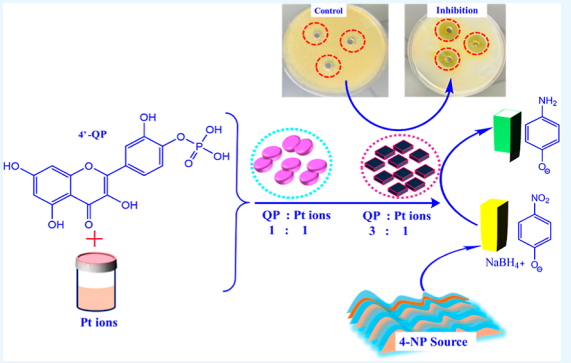

1. INTRODUCTION

Cumulative evidence shows that hospital technologies and surfaces are vehicles for the spread of nosocomial infections (e.g., urinary tract diseases) caused by drug-resistant *Citrobacter freundii*. Antibacterial surfaces and antibiotic (Metronidazole) treatment regimens against *C. freundii* are ineffective due to advances in bacterial resistance.[1−4] Conventional nanomaterials are typically prepared by physical and chemical methods using cetyltrimethylammonium bromide and nonaqueous organic solvents. These conditions raise toxicity and environmental safety concerns. For instance, the synthesis of PtNPs typically involves high temperatures (160−200 °C) with extended incubation periods and reducing agents such as sodium borohydride -$NaBH_4$ and organic capping agents.[5] $NaBH_4$ is a potential source of caustic salt and flammable gases. These reagents, while effective in controlling morphology during synthesis, promote catalyst poisoning. The synthesis of the nanoparticles must be altered to feature green reagents and to combat catalyst poisoning and degradation.[6] Eco-friendly nanosynthesis has been reported for platinum, gold, silver,[7,8] and copper nanoparticles,[9] with some acting as antimicrobials without the need for harsh conditions.[10]

The use of derivatized Quercetin (3,3′,4′,5,7-pentahydroxyflavone) as a water-based reducing and sequestering agent may create the preparation of sustainable nanosynthesis, allowing low-temperature nanodesigns. Green sustainable anisotropic platinum nanoparticles have been produced in this work using water-soluble 4′-QP. The rational control of sizes, morphology, and shape of metal nanoparticles is dependent on the choice of solvent, the nature of the reducing agent, reaction time, and mechanism. Several reports have demonstrated the controlled synthesis of metal nanoparticles of different sizes and shapes using plant extracts.[11] For instance, Lin and co-workers attributed the synthesis of cubic anisotropy of PtNPs to water-soluble hemicellulose extract.[12] In their work, the presence of hydroxyl functionality was believed to stabilize the cubic shape of the nanomaterial. In our case, phosphate, and hydroxyl functional groups of 4′-QP are hypothesized to aid its solubility and inherent reduction of platinum ions and stability in the synthesis of nanopeanuts and cubic platinum nanoparticles at room temperature. Platinum nanoparticles possess excellent catalytic activity, high stability, medicinal, and

Received: April 24, 2024
Revised: June 26, 2024
Accepted: July 1, 2024
Published: August 30, 2024

antimicrobial properties due to their intrinsic physicochemical tunable abilities (high surface area-to-volume ratio).[13,14]

Para-nitrophenol (4-NP) is a soluble EPA (Environmental Protection Agency) priority pollutant in industrial wastewater and surface water with carcinogenic effects that endanger human health. Biological, physical, and chemical techniques have been reported for the remediation of 4-NP, but these have been limited by low efficiency. The catalytic reduction of 4-NP to form a reusable 4-AP using a green nanocatalyst has become a reliable and efficient technology for environmental remediation.[15] Various catalysts such as AuNPs, PdNPs, and PtNPs have been reported to reduce 4-NP owing to their sizes.[15] Among the experimented catalysts for 4-NP reduction, PtNPs show an outstanding catalytic activity.[13]

We hereby demonstrate that 4′-QP shows an improved aqueous solubility and resists the typical oxidation of the catechol moiety of the B ring of quercetin (Scheme S1) into *o*-quinone at room temperature. Additionally, 4′-QP acts as a multifunctional reducing and stabilizing agent for the synthesis of monodispersed anisotropic greener platinum nanoparticles for controlling *C. freundii* and for the catalytic transformation of 4-nitrophenol in surface water. We focus on the shape-dependent effects of PtNPs on the reduction of 4-NP into environmentally safe and reusable 4-amino phenolate products. The characterization of anisotropic PtNPs using UV−vis spectroscopy, TEM, and XRD, energy-dispersive X-ray (EDX) confirmed the physicochemical properties, such as the sizes, composition, and morphology of the nanoparticles. The Cubic-PtNPs (C-PtNPs) and Peanuts-PtNPs (P-PtNPs) are applied as bacteriostatic agents against *C. freundii* in dose-dependent and kinetic assays. The bactericidal impacts of anisotropic PtNPs on *C. freundii* was visualized and confirmed using SEM. Kinetic assessment of C-PtNPs and P-PtNPs treatments on *C. freundii* were 99.7 and 77%, respectively. Shape-induced toxicity and excellent performance of C-PtNPs were attributed to high surface-to-volume ratio, highly energized active facets {111}, and sharp edges of nanocubes. This study demonstrated that sharp edges and distinct reactive faces of nanocubes contribute to the development of effective antimicrobials and catalytic enhancement.

2. EXPERIMENTAL SECTION

2.1. Materials. Platinum(II) chloride ($PtCl_2$) was purchased from Sigma-Aldrich, Milwaukee, WI. Quercetin was purchased from Indofine Chemicals Inc. (Hillsborough, NJ). All reagents were analytical grade purity unless stated otherwise. Ultrapure water with a specific resistivity of >18 MΩ cm was used to prepare all reagents. *C. freundii* ATCC 8090 was purchased from the American Type Culture Collection (ATCC) (Manassas, VA, USA). Muller Hinton (MH) media were purchased from Sigma-Aldrich (St. Louis, MO, USA). Sodium chloride (NaCl), sulfuric acid (H_2SO_4), and sodium hydroxide (NaOH) were purchased from Sigma (St. Louis, MO).

2.2. Instrumentation. Ultraviolet−visible (UV−Vis) measurements were recorded using an Agilent multicell Cary 3500 workstation. TEM and SEM measurements were performed on a JEOL TEM 2100F and JEOL SEM 7900F, respectively. The TEM sample preparation for PtNPs entails drop-casting an aliquot of the supernatant layer from centrifugation to a new SiO_2-coated 300 mesh copper grid. The TEM images of PtNPs and their size distributions were plotted. Elemental platinum was determined by an EDX analyzer. The XRD measurement was performed using a Bruker D8 Discover XRD system operated at 40 kV. The XRD samples were dried and mounted on a sample holder for measurements. Furthermore, XRD patterns were obtained with an X-ray diffractometer equipped with Cu−Kα radiation. The scanning was performed at a 2-theta angle over the range of 5 to 80°.

2.3. Synthesis of Quercetin 4′-Monophosphate (4′-QP). 4′-QP was synthesized to enhance the polar solubility of Quercetin in our previous work.[16] The synthesis entails the selective substitution of the OH group at position 4′ on Quercetin with an inorganic phosphate group. To this effect, the parent quercetin compound was protected using dibenzyl phosphite except at the 4′ position. Selective phosphorylation of the 4′ position on Quercetin ($C_{15}H_{10}O_7$) was performed to achieve 4′-QP following a reported synthetic pathway with detailed structural characterization. The details of the synthesis are reported elsewhere.[16]

2.4. Synthesis of Anisotropic PtNPs. Monodispersed anisotropic platinum nanoparticles were prepared by a simple chemical reduction method. The nanoparticles were generated via the reduction of $PtCl_2$ by 4′-QP in water without additional surfactants. In a one-pot synthesis, 0.01 M $PtCl_2$ reacted with 0.05 M 4′-QP in the molar ratios of 1:1, 2:1, and 3:1, respectively. The reaction was further exposed to 50 °C heat incubation for 1 h to ascertain any changes in the resultant shape of nanopeanuts (T1-T2) (Table 1). Next, Cubic PtNPs were synthesized by keeping the concentration of the platinum metal precursor (0.01 M $PtCl_2$) constant and varying the concentration of 4′-QP (0.05 M) at 1:1, 1:2 and 1:3, respectively (P1−P3). C-PtNPs were synthesized without heat. Table S1 shows the synthesis of anisotropic PtNPs.

Table 1. Average Zone of Inhibition after PtNPs Treatment of *Citrobacter freundii* between 0 and 5 days of Incubation

Bacteria	Treatment Concentration (μg/mL)	Zone of Inhibition (mm)	
		P-PtNPs	C-PtNPs
Citrobacter freundii	20	0.00 ± 0.00	6.40 ± 0.10
	40	1.00 ± 0.05	9.75 ± 0.15
	60	4.50 ± 0.15	16.28 ± 0.10

2.5. Preparation of *C. freundii*. Bacteria cultures were prepared by following an aseptic National Committee for Clinical Laboratory Standards (NCCLS) standard procedure.[17] MH Agar was prepared using the manufacturer's recommendation.[18] Briefly, 3.8 g of MH powder was dissolved in 100 mL ultrapure water. The homogenized agar mixture was then autoclaved at 121 °C for 30 min. MH broth was prepared in a similar procedure. Freshly prepared MH agar solution was spread-plated into a 100 mL sterile Petri dish to form solid media. To prepare the bacteria culture, 10 μL of the stock culture was inoculated into 9 mL of MH broth, and the culture tubes were transferred into a 35 ± 1 °C Thermo Scientific Heratherm incubator for 24 h. After incubation, 75 μL of *C. freundii* from the working culture were inoculated into a fresh MH broth, incubated at 35 ± 1 °C, and harvested during the exponential growth phase by centrifugation. The supernatant was discarded, and the bacteria were resuspended in PBS pH 7. The bacteria concentration at 600 nm (OD_{600}) was measured

https://doi.org/10.1021/acsomega.4c02948
ACS Omega 2024, 9, 38557−38568

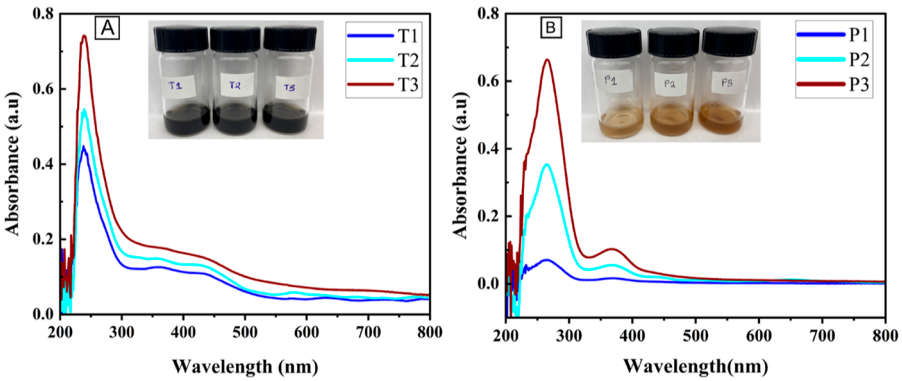

Figure 1. (A) UV−vis absorption spectra for the synthesis of P-PtNPs (B) synthesis of Platinum nanocubes. Inset: reaction vials containing varying amounts of 0.05 M 4′-QP and 0.01 M $PtCl_2$.

using a UV−Vis spectrophotometer and further adjusted to 10^{-6} CFU/mL using a hemacytometer.

2.6. In Vitro Antibacterial Test. The shape-dependent antibacterial activity of anisotropic platinum nanoparticles was tested on *C. freundii* using the agar well diffusion method.[19,20] Bacteria suspension made of 10^{-6} CFU/mL was seeded onto the freshly prepared MH agar plates. Three holes equidistant from each other were created using a cork borer, and successive concentrations of 20, 40, and 60 μg/mL of anisotropic PtNPs were pipetted into the wells of each agar plate. 4′-QP was used as a control. The bacteria-inoculated plates treated with the PtNPs were incubated at 35 °C. The agar plates were assessed daily within a 72 h incubation period. The zone of inhibition was measured with specific intervals for 3 days, and the average results were expressed in millimeters (mm). The experimental setup was performed for both cuboidal and peanut PtNPs under aseptic conditions. The minimum inhibitory concentrations (MIC) was determined by the standard broth microdilution method (Supporting Information).

2.7. Time Killed Evaluation of Shape-Dependent PtNPs against *C. freundii*. To determine the shape effects of C-PtNPs and P-PtNPs on *C. freundii* with respect to time, UV−vis measurements (OD_{600}) were performed on bacterial cells (log phase) treated with 60 μg/mL of P-PtNPs and 60 μg/mL of C-PtNPs in separate culture tubes. The control tube received 4′-QP as the treatment. The tubes were incubated on a shaker at 35 °C for 24 h, and the OD_{600} values were measured at an hourly interval using an Agilent UV−vis Cary 3500. The bacterial viability was quantified and calculated according to the following formula.

$$\%\ D\ (\text{percent viability}) = (D'_{600} - D_{600})/(D'_{600}) \times 100$$

where % D stands for percent viability, the D'_{600} is the control, and the D_{600} represents the treated bacterial cells.

2.8. SEM Characterizations of *C. freundii*. To visualize the shape influence of C-PtNPs on bacterial cells, the bacteria cells in MH broth media were treated with 25 μg/mL (MIC) of C- PtNPs and incubated at 35 °C for 24 h contact time. The SEM sample preparation adapted for visualization is as follows: the C-PtNPs-treated bacteria were harvested by centrifugation at 5000 rpm for 5 min. The precipitate was prepared for SEM visualization by washing with PBS 3×, followed by the fixation with 2.5% glutaraldehyde for 6 h at 4 °C. After the glutaraldehyde was discarded, the bacteria cells were dehydrated using a different grade of the ethanol mixture in a sequential manner of 0, 50, 70, 90, 95, and 100%. Finally, the bacteria cells were harvested and freeze-dried for the SEM investigation.

2.9. Catalytic Activity of Anisotropic PtNPs on 4-NP in Wastewater Samples. Grab wastewater samples were obtained from an anonymous waste plant in Middlesex County, New Jersey, following EPA method 537.1. The physical characteristics of the water samples include pH 6.8 and colorless solution to avoid interference in the analysis of 4-NP. The kinetic reduction of 4-NP in the presence of a PtNPs catalyst was monitored at room temperature to determine the shape-dependent catalytic properties of C-PtNPs and P-PtNPs. In a typical catalytic experiment, 1 mL of wastewater spiked with 10^{-4} M 4-nitrophenol was mixed with 0.5 mL of 0.1 M sodium borohydride solution and diluted with 10 mL deionized water. The catalytic reaction was initiated by the addition of 50 μL PtNPs catalyst in a cleaned quartz cuvette at 25° (room temperature). A UV−Vis spectrophotometer was used to record the time-dependent absorption spectra over the wavelength range of 250−550 nm.

2.10. Statistical Analysis. The experiments were performed in triplicates, and all the data are expressed as the mean ± standard deviation from the successive experiments. The data in this study were subjected to statistical analysis of one-way ANOVA using Origin Pro Software. A probability ($p < 0.05$) was considered statistically significant.

3. RESULTS AND DISCUSSION

3.1. UV−Vis Characterization of Cuboidal and Peanuts Platinum Nanoparticles. UV−vis measurements were performed to monitor the formation of anisotropic PtNPs at room temperature within the wavelength range of 200−800 nm. Quercetin Monophosphate (4′-QP) (Figure S1) acted as the reducing and capping agent for the reduction of Pt^{2+} ions in water. The UV−vis spectra of unmodified quercetin exhibit two major absorption bands. The first absorption band I at 370 nm is ascribed to the B ring cinnamoyl system, while the second band II at 256 nm represents the A ring benzoyl system.[21,22] In the case of 4′-QP, a new absorption band appeared around 274 nm (band II) and a less pronounced peak at 375 nm (Figure S3) due to the presence of phosphate group at the 4′ position of quercetin. Figure 1 shows the UV−vis spectra of C-PtNPs and P-PtNPs with different molar concentrations of 4′-QP and $PtCl_2$ reactants. The broad SPR absorption peak from 320 to 400 nm in Figure 1A indicated the formation of platinum nanoparticles (Inset: reaction vails

https://doi.org/10.1021/acsomega.4c02948
ACS Omega 2024, 9, 38557−38568

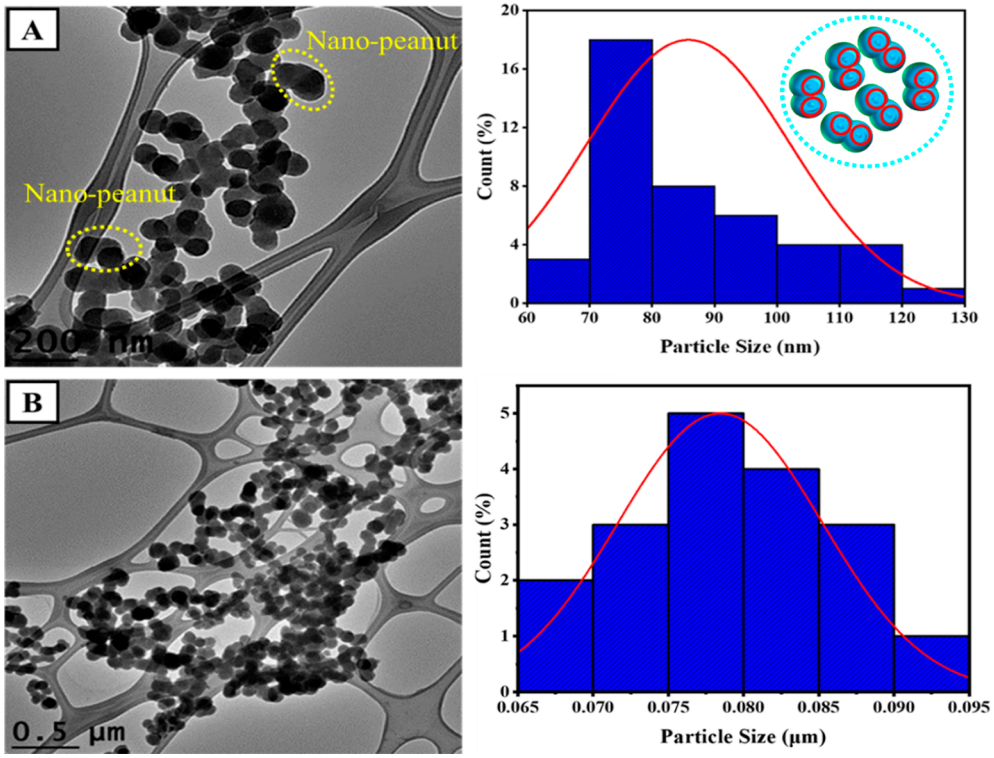

Figure 2. (A-B) HRTEM images of P-PtNPs with sizes 39.1 ± 0.20 nm and 43.11 ± 0.12 nm, respectively. Inset: schematic model of PtNPs.

T1−T3). Similar studies show that the SPR peak of platinum nanoparticles is broad over the range of 215−370 nm,[23] which confirms our results. Phytochemical agents (flavonoids) composed of hydroxyl functional groups are responsible for the reduction of Pt^{2+} to Pt^0. In this study, the phosphate and hydroxyl groups of 4′-QP are electron-rich sites that form a complex with Pt ions, thus facilitating the reduction of Pt ions during the nucleation of PtNPs. The concentration-dependent effect of water-soluble 4′-QP on the reduction rate of Pt ions in solution was investigated to determine the physicochemical properties of resultant anisotropic platinum nanoparticles. In a typical experiment, 4′-QP was reacted with Pt ions in a molar ratio of 1:1, 1:2, 1:3, respectively. In this setup, the 4′-QP acts as the limiting reagent in the presence of the increasing concentration of the Pt ions. Since 4′-QP is limited, Pt ions are not completely reduced, and the reduction rate is slow, with limited growth of nanoparticles after the nucleation stage. It is worth noting that as the reactant concentrations increase, the absorbance of the nanoparticles increases.

In the second experiment (Figure 1B), the effect of increasing 4′-QP in the presence of a fixed concentration of Pt ions was investigated. The increasing effect of 4′-QP in the presence of platinum metal precursor in the molar ratio 3:1 shows the reduction power and shape-directing property of 4′-QP, respectively. Excess 4′-QP acting as both reducing and stabilizing agents further directed the resultant shape of the nanoparticles. It was observed that the 2:1 ratio gives a mixture of cubes and irregular shapes. The 3:1 ratio of 4′-QP and Pt ions gives a monodispersed and uniform cubic shape. Experimental evidence has shown that the decrease in particle size correlates to the increasing reducing agent.[23] This phenomenon is attributed to the increased reaction rates due to excess reducing agents during the nanosynthesis. When the reaction rate increases due to the high concentration of the reducing agent, the platinum ions are rapidly reduced, which leads to smaller particles.

The UV−vis spectra exhibit a sharper SPR peak, indicating the formation of smaller particles upon increasing reducing agents. This observation has been reported in similar studies elsewhere.[23,24] Furthermore, the synthesis of PtNPs was exposed to 50 °C heat treatment to identify the optimum temperature for the shape evolution of the nanoparticles. The color of the nanoparticle solution became dark, as seen in Figure 1A inset (T1−T3). The influence of heat treatment (50 °C) increased the kinetic reaction of nanoparticles to form nuclei that further grow into matured PtNPs. It was observed that increasing the heat (>50 °C) rapidly increased the reaction kinetics and vice versa. In all, the rate of heat treatment impacts the nucleation process and modulates the sizes of the resultant PtNPs, without altering the shape.[25]

3.2. TEM Characterization of Anisotropic PtNPs. The morphological characterizations of the as-synthesized anisotropic platinum nanoparticles were performed with high-resolution TEM.[26] Figure 2A shows the TEM image of prepared nano peanuts. The formation of nanopeanuts are highly dense uniform particles possessing smooth surfaces. The as-prepared nanopeanuts are composed of two or more interconnected growing particles produced via aggregation of smaller spherical nanoparticles.[27] It is worth noting that increasing the Pt metal precursor to 4′-QP in the ratio of 2:1 and 3:1 led to the formation of the nanopeanuts.

In Figure 2A, the interparticle lattice fringes were estimated to be 0.22 nm, which reveals that the growth and crystallinity of the nanoparticles occur preferably on the (111) index plane.[27] To investigate the increasing effect of 4′-QP on the reduction of Platinum ions, the molar ratio of 4′-QP to $PtCl_2$ reactants was maintained at 2:1, and the resulting particles

https://doi.org/10.1021/acsomega.4c02948
ACS Omega 2024, 9, 38557−38568

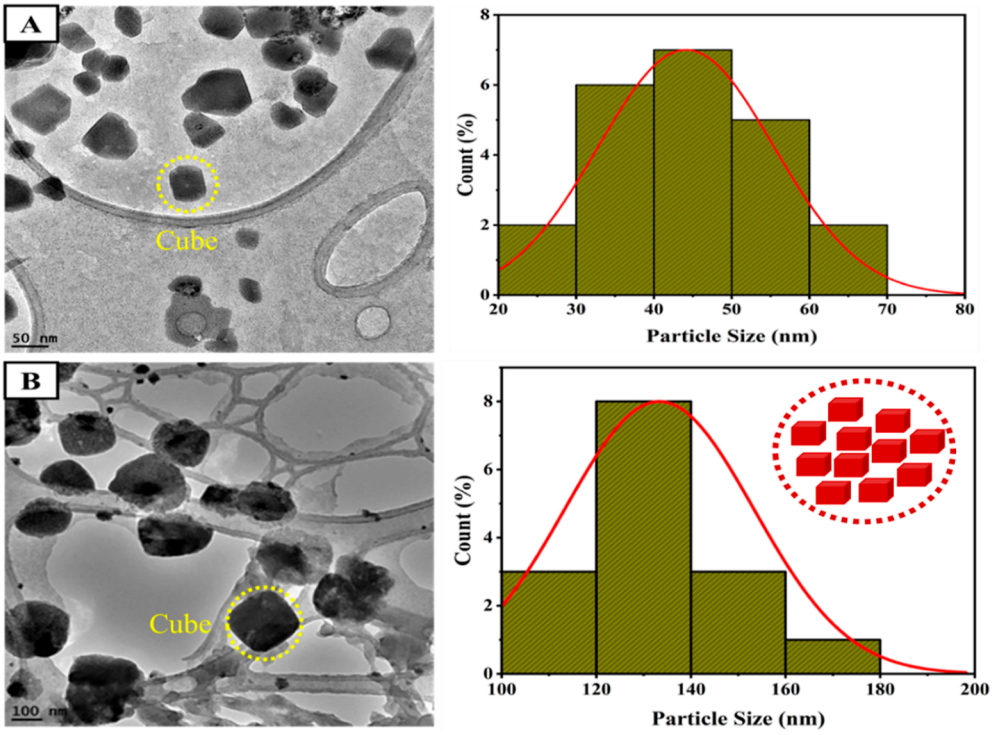

Figure 3. (A) HRTEM image of irregular-shaped anisotropic PtNPs with the corresponding size distribution histogram. (B) C-PtNPs at 25 °C. Inset: a schematic model of nanocubes. The mean size of (A,B) were 45.1 ± 0.24 and 48.1 ± 0.17 nm, respectively.

adopted irregular anisotropic shapes such as cubes and cuboidal shapes as seen in Figure 3A.

To achieve and confirm the platinum nanocubes, the molar concentrations of 4′-QP and Pt^{2+} ions were fixed at 3:1, respectively. The high concentrations of 4′-QP reacting with the low concentrations of Pt^{2+} ions led to the formation of platinum nanocubes (Figure 3B). The concentrations of the 4′-QP (shape-directing agent) and $PtCl_2$ were maximized to achieve different shapes and sizes. Figure 3B shows that the nanocubes are monodispersed with smooth edges. The clear lattice fringes reveal the crystallinity of the particles which is represented by the sharp peak of {111} index.[26] The data suggest that the morphology of nanoparticles can be tuned and controlled with an increasing reducing/stabilizing agent (4′-QP) concentration with respect to a lower concentration of metal precursor. The significant effect of reducing, capping, and stabilizing agents on the shape and size of platinum nanocubes is justified by the concentration variations of the 4′-QP and $PtCl_2$ reactants. It is plausible that the coordination between Pt^{2+} ions and 4′-QP plays a role in stabilizing the resultant particles. The particle mean sizes from the size distribution histogram were determined by measuring nanoparticles in different sections of the TEM grid. The monodispersed platinum nanocubes exhibit a mean size of 45.1 ± 0.24 and 48.1 ± 0.17 nm for Figure 3A-B, respectively.

3.3. Growth Mechanism of Shape-Controlled PtNPs.

The concentration effects of 4′-QP on the shape evolution of anisotropic platinum nanoparticles were studied using a time-dependent UV−vis absorption spectroscopy. In a typical particle growth experiment, 3 mol equiv of 4′-QP were reacted with 1 mol equiv of Pt ions stirred at 100 rpm. Figure 4 shows the absorbance measurements at a 10 min fixed time interval starting from time, *t*-0, to *t*-80. The different shapes observed with changing concentrations can be understood by the growth

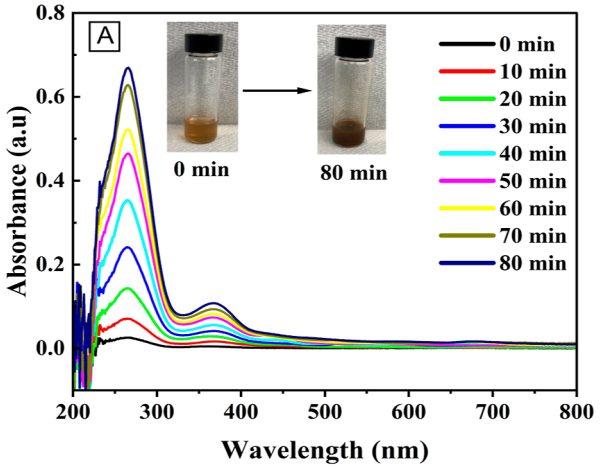

Figure 4. Time-dependent formation of cubic PtNPs at room temperature from time t_0 to t_{80}.

mechanism of the platinum particles.[26,28] When low 4′-QP concentrations reacted with Pt^{2+} ions, the rate of platinum nucleation was slow. The 4′-QP acting as the reducing and capping agent played the role of limiting reagent. The resultant nuclei grow into a spherical shape. It was observed that the platinum nanoparticles agglomerate and further grow into nanopeanuts. The energetics of the platinum ions and 4′-QP are the driving force for shape evolution under a low concentration of 4′-QP. Nevertheless, a different growth mechanism occurred when a higher concentration of 4′-QP reacted with Pt^{2+} ions.

Since the concentration of 4′-QP is high, the reduction of Pt^{2+} ions occur rapidly, resulting in a faster growth of the anisotropic platinum nanoparticles. In addition, the kinetic control of the growth mechanism was favorable when the 4′-

https://doi.org/10.1021/acsomega.4c02948
ACS Omega 2024, 9, 38557−38568

Scheme 1. Growth Mechanism of the Shape-Controlled Process of Platinum Nano-Peanuts and Nanocubes

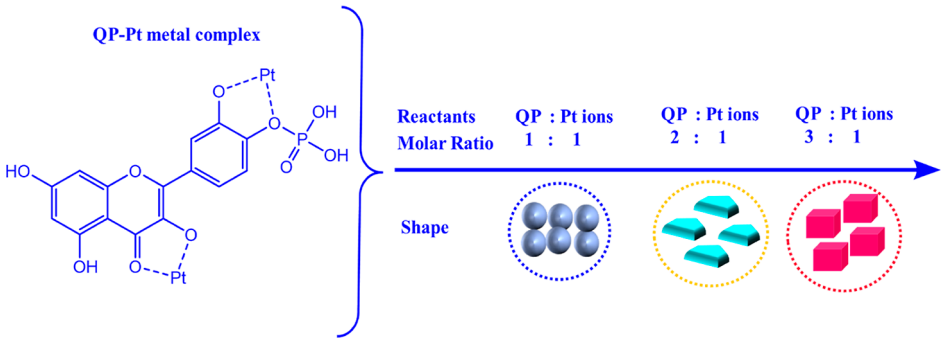

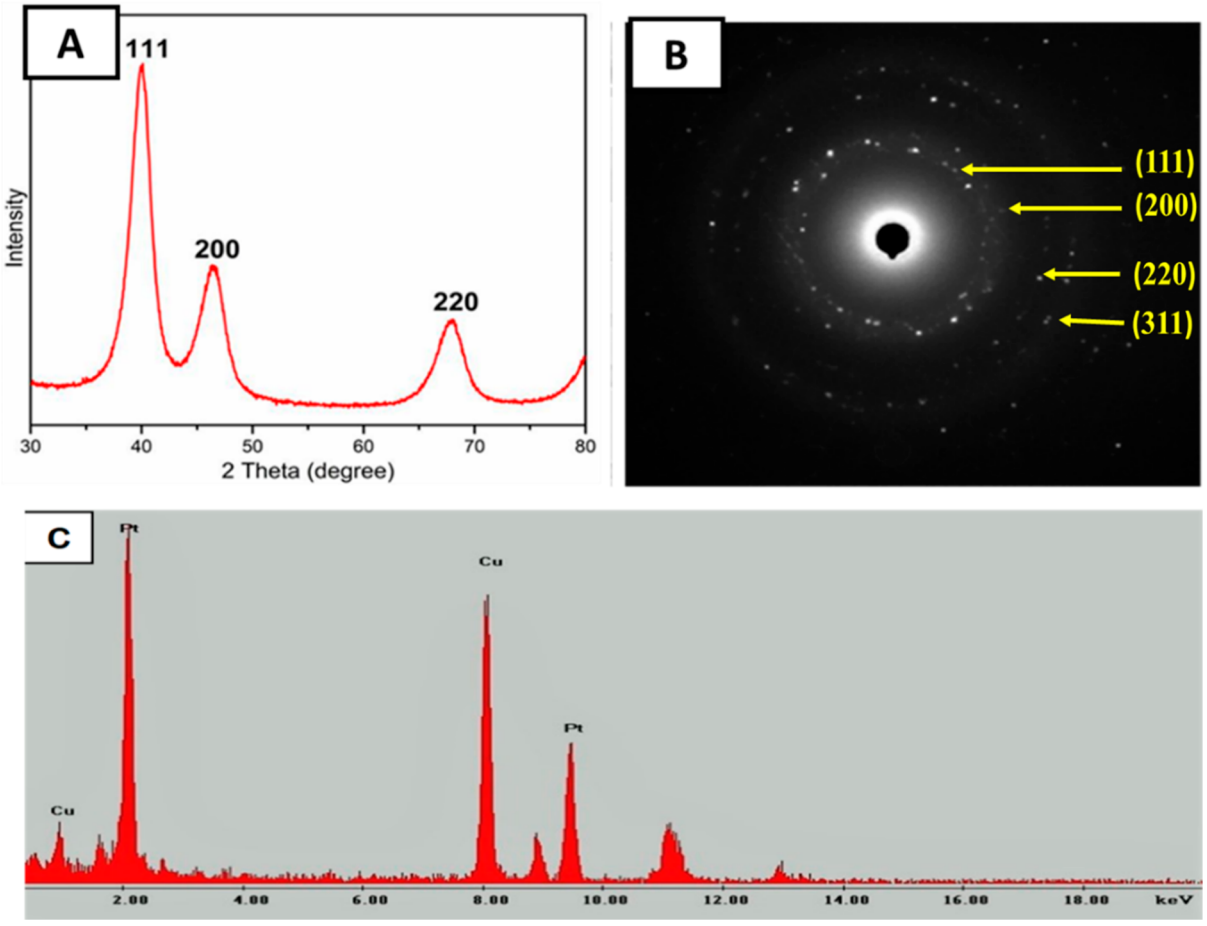

Figure 5. (A) XRD of anisotropic PtNPs. (B) SAED (C) EDX.

QP was in excess. Preferentially, the growth of particles occurred at the {1,1,1} index plane of the nuclei;[27,28] hence, the reduction rate of Pt^{2+} ions directs the final shape of the particles. The growth of platinum on the {1,1,1} index has been attributed to the influence of surfactants, which can change the growth kinetics of the resultant particles. Some reports have shown that synthetic nanoparticle reactions under kinetic growth produce anisotropic particles such as highly branched particles.[26,28] In summary, the mechanism of nanocube formation follows (i) nucleation, thus reduction of Pt^{2+} ions transitions into the nuclei, (ii) rapid growth processes at high concentrations of 4′-QP (iii) directional growth of nanocubes particles.[28] The schematic representation of the growth mechanism of anisotropic platinum nanoparticles is shown in Scheme 1.

3.4. XRD Characterization. XRD analysis was performed to characterize the crystal structure of as-synthesized anisotropic PtNPs. In Figure 5A, the XRD pattern confirmed the PtNPs crystal structure. The three distinct peaks at 40.12, 46.70, and 67.89° over the 2-theta range of 30−80° were ascribed to {111}, {200}, and {220} index planes, respectively. The characteristic peaks represent face-centered cubic (FCC), which agree with reported data and the Joint Commission on Powder Diffraction Standards (JCPDS:004-0802).[27,29] The most intense peak and preferred growth of the platinum nanoparticles is along the {111} plane.[23,29] The energy dispersive (EDX) X-ray analysis revealed the elemental signal

https://doi.org/10.1021/acsomega.4c02948
ACS Omega 2024, 9, 38557−38568

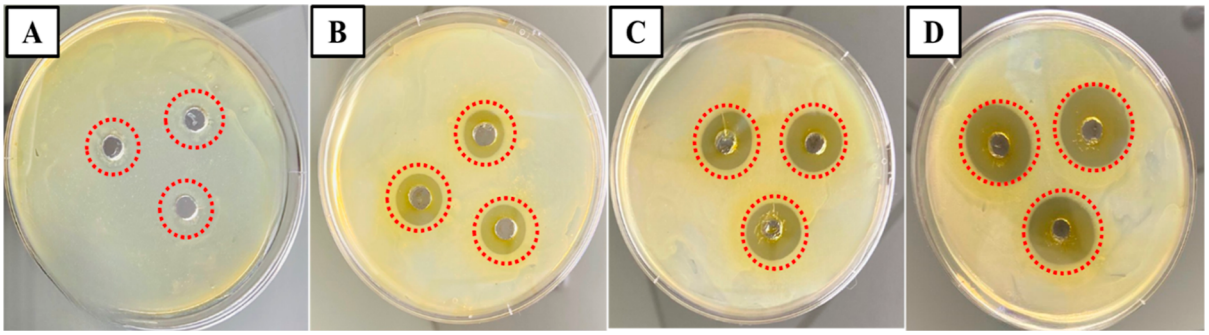

Figure 6. Dose−response inhibition of *C. freundii* in the presence of C-PtNPs (A) Control (B) 20 (C) 40 (D) 60 μg/mL. The control group was treated with 4′-QP and did not show any zone of inhibition. Each concentration was repeated in triplicates.

of platinum, as shown in Figure 5C. The elemental composition of the PtNPs shows a sharp and intense peak at 2.2 keV, corresponding to the presence of Pt. The copper peak at 8 keV originates from the copper grid on which the sample was coated. The selected area electron diffraction (SAED) pattern shows a ring formation and sharp diffraction spots from the anisotropic Pt nanoparticles. The SAED ring pattern (inner to outer) is assigned to the {111} and {220} index reflections of the FCC of nano platinum, respectively (Figure 5B). The SAED confirms the crystallinity of the as-synthesized PtNPs. Our results agree with reports by Venu et al.[29]

3.5. Antibacterial Performance of Shape-Dependent PtNPs against *C. freundii*. The shape dependency activity of P-PtNPs and C-PtNPs was tested on *C. freundii* as the model microorganism due to its nosocomial infections (urinary tract diseases) by using the agar well diffusion method, as seen in Figure 6. The shape effects of PtNPs treatments were assessed using a zone of inhibition method for 5 days. To investigate the influence of shape on the antibacterial performance of P-PtNPs and C-PtNPs, the synthetic routes, concentrations, and selected average sizes of both nanoparticles were kept constant at approximately 45.1 ± 0.24 nm. Three agar plates seeded with *C. freundii* (10^{-6} CFU/mL) were treated with 20, 40, and 60 μg/mL of C- PtNPs in a dose-dependent manner. This experimental setup was repeated for the treatment of P-PtNPs. Figure 6 shows the results after the treatment of C-PtNPs against *C. freundii.* At 20 μg/mL treatment of C-PtNPs, a visible zone of inhibition (6.40 ± 0.10 mm) is observed. The inhibition zone increases with an increasing dose treatment of C-PtNPs. However, the dose treatment of the P-PtNPs did not show tangible zone of inhibition at 20 μg/mL (Figure S4). Meanwhile, the zone of inhibition of 1.00 ± 0.05 and 4.50 ± 0.15 mm was observed for P-PtNPs at 40 and 60 μg/mL, respectively. At a constant dose, the antibacterial performance of C-PtNPs is higher than P-PtNPs.

The excellent antibacterial activity of the C-PtNPs can be ascribed to the contact interaction and active facets as the two important factors that drive the antibacterial effectiveness of the nanoparticle shape. Furthermore, the high surface-to-volume ratio of the nanocubes binds strongly to the cell membrane of *C. freundii* in comparison to P-PtNPs. The performance of nanocubes is ascribed to the sharp edges and high-energy active facets {111} that demonstrate stronger reactivity.[30] Antimicrobial studies on the facet reactivity of nanoparticles have been demonstrated by Ren et al.[31] Furthermore, shape-dependent studies of silver nanoparticles have been demonstrated by Pal et al.[32] Their results showed that triangular nanoplates of Ag induces a higher antibacterial activity owing to the active facet of nanosilver as compared to spherical silver.[32] Our findings suggest that the as-prepared C-PtNPs interact with the bacterial cell surface via contact killing and arresting the growth of the *C. freundii* via inducing membrane damage. The effectiveness of PtNPs was confirmed by determining the MIC against *C. freundii*. The C-PtNPs nanoparticles exhibit a MIC value of 25 μg/mL, while the MIC of P-PtNPs was 45 μg/mL (Figure S5) against the *C. freundii.* In all, the C-PtNPs are more effective compared to P-PtNPs, supporting the evidence that the morphology and small surface-to-volume ratio influences the bactericidal activity of C-PtNPs against *C. freundii.*[33,34] We found that the inhibition zones of C-PtNPs at low concentration against *C. freundii* can exert a bactericidal effect inhibiting the growth of the bacteria as compared to the P-PtNPs. For stability and effectiveness of the C-PtNPs,[35] the dose-dependent inhibition was repeated three times, and it was observed that there was no bacteria growth in the zone of inhibition for several days. The C-PtNPs interacted highly with the bacteria, as indicated at the edges of the zone of inhibition, suggesting that they released their toxins onto the agar plates. This result indicates that C-PtNPs nanoparticles target resistant bacteria via the release of the ion via contact killing, and this approach could be a promising therapeutic agent to eradicate emerging microbial resistance.[4,34] Table 1 shows the average zone of inhibitions and demonstrates that the as-prepared anisotropic PtNPs possessed potent bactericidal activity compared to the controls. This study demonstrates the potential of the anisotropic PtNPs against *C. freundii*resistant bacteria.

3.6. SEM Characterization of PtNPs Treated *C. freundii*. Visualization of bacteria morphology was performed using SEM to ascertain the inhibitory effects of C-PtNPs on bacteria cell membranes since C-PtNPs were more effective than P-PtNPs. The experimental setup included *C. freundii* treated with C- PtNPs at MIC of 25 μg/mL and the control experiment did not receive treatment. The experimental setups were incubated at 35 °C for 24 h contact time. After this step, the bacteria cell samples were prepared for the SEM analysis following a standard procedure.[36]

Figure 7A shows the bacteria control cells maintained an intact rod-like shape in the absence of PtNPs treatment. Nonetheless, it was observed that the bacterial cell membrane suffers structural damage after exposure to C-PtNPs in Figure 7B. The bacterial cells were deformed, indicating severe membrane damage followed by cell contents released into the media with a loss of their intact rod-like shape. It can be observed that 25 μg/mL of the C- PtNPs coat the surface of the *C. freundii*, thus the coating of PtNPs on bacteria cells

https://doi.org/10.1021/acsomega.4c02948
ACS Omega 2024, 9, 38557−38568

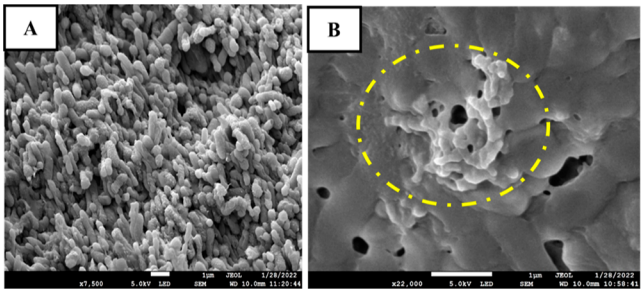

Figure 7. SEM images of PtNPs treated *C. freundii*. (A) Control (B) C-PtNPs at 25 μg/mL.

established an effective interaction via the active facets of platinum nanocubes. The C-PtNPs coating on *C. freundii* demonstrated the inhibitory effectiveness of cubic PtNPs and initiated cell death.[36]

3.7. Kinetic Assessment of Shape-Dependent PtNPs on *C. freundii*. The growth inhibition curves of *C. freundii* after contact with shape-dependent PtNPs are shown in Figure 8A. The treatment of C-PtNPs showed a significant time-dependent decrease in the viability of bacteria cells from 10^6 to 10^1 CFU/mL after 24 h incubation. The PtNPs poison the media via platinum ion migration, this effect coats the surface of the bacteria membrane, thus inhibiting its growth. This indicates the bactericidal action of anisotropic PtNPs. The inhibitory effect of C-PtNPs on *C. freundii* was more pronounced than P-PtNPs.

Furthermore, the Spread-plate technique was adopted to confirm the contact killing of *C. freundii* in broth media in the presence of anisotropic PtNPs. Briefly, *C. freundii* in broth media treated with or without P-PtNPs (60 μg/mL), and C-PtNPs (60 μg/mL), were incubated at 35 °C for a 24 h contact time. After this step, the treated and untreated *C. freundii* were plated on a freshly prepared agar to confirm the contact killing of the bacteria. Figure 8B−D confirms the shape−effect activity of C-PtNPs and P-PtNPs on *C. freundii* after the kinetic assessment from contact killing. Bacteria colonies were counted to determine the inhibition rate of PtNPs. Figure 8C,D shows inhibition rates of 99.7 and 77% for C-PtNPs and P-PtNPs, respectively.

The shape effect of C-PtNPs shows a higher kinetic antibacterial activity than P-PtNPs because the nanocubes possess sharp edges and active facets[30] responsible for high bactericidal activity against *C. freundii*. Taken together, C-PtNPs kill *C. freundii* faster and more effectively than P-PtNPs due to its morphology given that the antibacterial factors such as particle sizes, and concentration are controlled and constant. Hence, the particle shape could be an essential parameter in the design of time-dependent antibacterial agents. Our results agree with similar reports elsewhere.[19,37]

3.8. Mechanism of Bacterial Inhibition by Shape-Dependent PtNPs. The shape effects of PtNPs on bacteria cells are the main goal of this work. In this study, Peanut-shaped PtNPs are compared to cubic-shaped PtNPs for their antibacterial performance. Past Literature demonstrated that differences in the antimicrobial activity of nanoparticles are attributed to multiple factors such as size and shape.[30] Our results suggest that cubic shaped-PtNPs inhibit bacterial growth via a contact-killing mechanism due to active facets of nanocubes, and sharp edges of cubes that facilitate effective interaction with bacteria cell membrane in comparison to the nano peanut shape.[30] Furthermore, some of the bacteria mechanism of PtNPs involves the Pt ions coating and binding to cell membranes of microorganisms and affecting the protein machinery of bacterial cells.[38] The binding of Pt ions to the bacteria membrane leads to the leakage and rupture of the bacteria cell membrane causing bacteria death. Some reports have demonstrated the bacterial inhibitory mechanisms, which include nanoparticle interference of DNA replication machinery and the induction of tumor suppressor proteins for a bacterial apoptosis-like response, reactive oxygen species, leading to bacteria death.[34,39] These findings agree with myriad studies suggesting that the physical and chemical parameters of the nanomaterials, such as dose, size, concentration, shape, and exposure time, influence the bactericidal activity of PtNPs.

Smaller concentrations of C-PtNPs were used as the biocidal agent to achieve sustainable bactericidal activity against *C. freundii*. Previous reports have shown that higher Pt concentration has toxic and detrimental effects on biological cells, limiting its therapeutic applications.[34,40] In our case, lower concentrations of PtNPs (20−60 μg/mL) showed excellent shaped dependent antibacterial potency with controlled physicochemical properties. We envision that PtNPs could serve as a bactericidal agent for the long-term treatment of a wide range of antibiotic-resistant microorganisms. The anisotropic PtNPs in this study demonstrate an eco-friendly nanomaterial with promising antibacterial activity at lower concentrations.

3.9. Shape-Dependent Catalytic Activity of PtNPs on Wastewater Samples. 4-NP is applied in the synthesis of

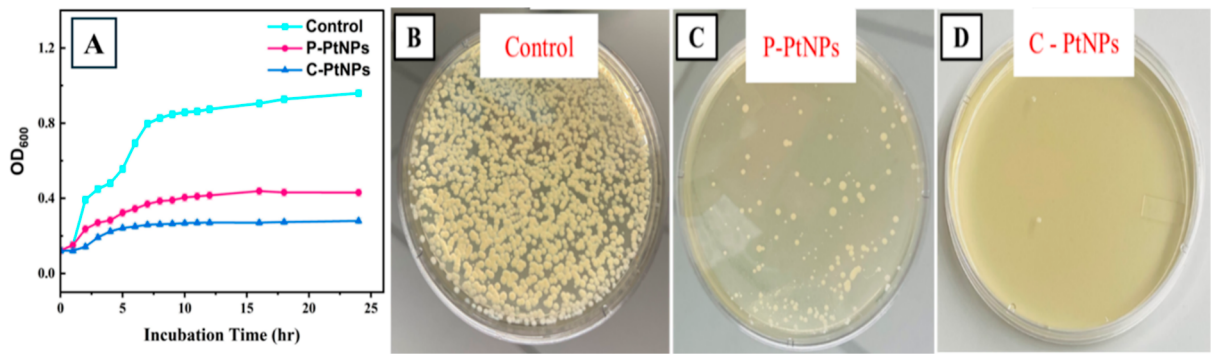

Figure 8. Time killed inhibition assessment of shape-dependent PtNPs treatments on *C. freundii* (A) UV−vis spectra (B) Control (C) P-PtNPs (60 μg/mL) (D) C-PtNPs (60 μg/mL). Concentration and sizes are kept constant to assess the effects of shape.

https://doi.org/10.1021/acsomega.4c02948
ACS Omega 2024, 9, 38557−38568

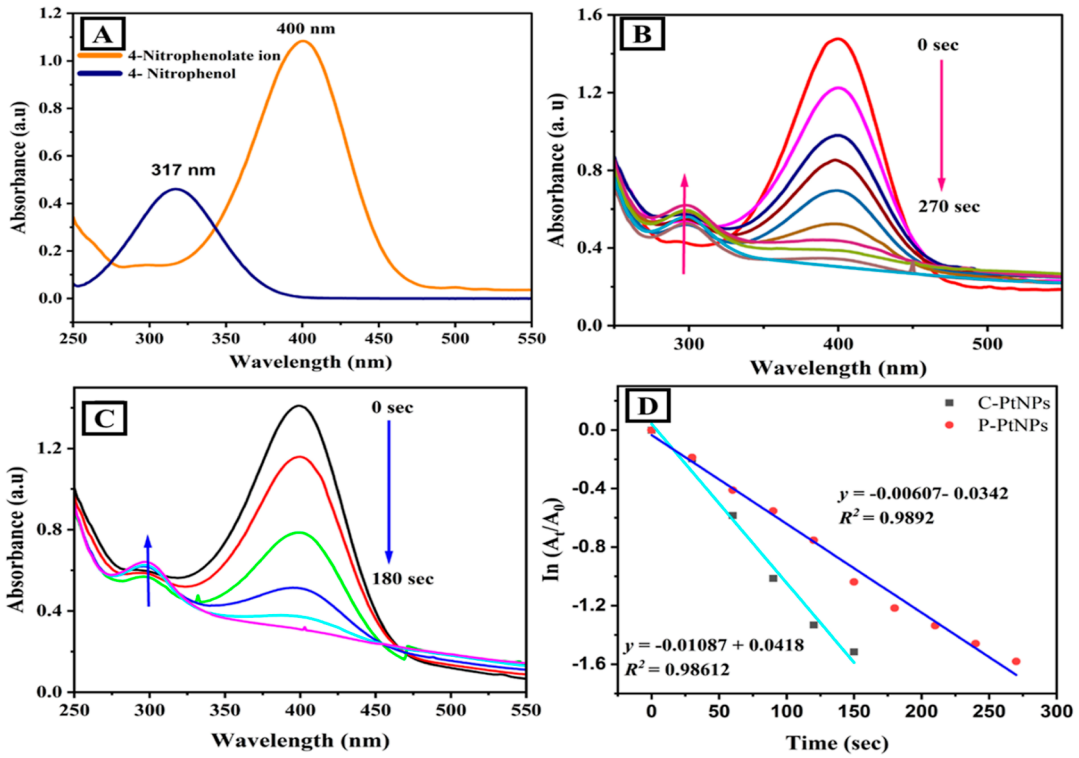

Figure 9. Absorption spectra of 4-NP conversion to 4-AP in the presence of Pt catalyst (A) control (B) P-PtNPs (C) C-PtNPs (D) plot of ln (A_t/A_o) vs time (s).

Table 2. Comparative Analysis of Shape-Dependent Activity of Different Nano-Catalyst

	Physicochemical parameter			
Nanocatalyst	Shape	Size (nm)	Degradation rate (k)	References
AuNP	cubes	45.1	0.00249 s^{-1}	Sundarapandi et al.[42]
PdNPs	cube	50	0.114 min^{-1}	Dang-Bao et al.[43]
AgNPs	hexagonal	43	0.259 min^{-1}	Khoshnamvand et al.[44]
AgNPs	quasi-spherical	36	0.265 min^{-1}	Yaun et al.[45]
PtNPs	Peanut	39	0.00607 s^{-1}	this study
PtNPs	Cube	43	0.0108 s^{-1}	this study

drugs and fungicides. New Jersey is one of the manufacturing hubs for pharmaceutical products. Pollution of surface water is a pressing problem in several superfund sites across New Jersey State due to accidental spills of organics and waste management problems. Surface waters in NJ are contaminated with toxic organics. Analysis of the reaction mixture of 4-nitrophenol (4NP) and anisotropic PtNPs catalyst was performed in a wastewater sample using sodium borohydride ($NaBH_4$) as a hydride source to determine the performance of the shape-dependent catalyst. For a standard catalytic reaction to progress, 4-NP was mixed with $NaBH_4$, and the resultant solution was deep yellow, which indicates the formation of 4-nitrophenolate anions with an absorption peak at 400 nm. In Figure 9A–C, excess $NaBH_4$ reacted with 4-NP concentration to ensure an ample supply of hydride ions for raising the pH and nitro group deprotonation to maintain a constant reduction rate of 4-NP concentration.[41] There was no observable change in the absorption peak at 400 nm in the absence of the PtNPs catalyst.[13] The addition of the catalyst initiates the catalytic reduction of 4-NP to form 4-AP with the evidence for the decreased absorption peak at 400 nm, simultaneously giving rise to the appearance of a new peak at 317 nm (4-AP).

The absorbance of each 4-NP reduction cycle was time-dependent, and a linear fitting of $-\ln (A_t/A_0)$ vs time (s) was plotted to determine the apparent rate constant (K_{app}).[41] (Figure 9D).

From the plot, the reduction of 4-NP followed the pseudo-first-order kinetics due to the excess $NaBH_4$ applied in the experiments. The apparent kinetic rate constant (K_{app}) was calculated from the slope of linear regression using eq 1

$$\ln(A_t/A_0) = -K_{app} \quad (1)$$

From the pseudo-first-order plots, K_{app} was estimated to be 0.00607 and 0.0108 s^{-1} for nanopeanuts and nanocubes, respectively. It was observed when experimental conditions (reactant concentration and nanoparticle sizes) for the reduction of 4-NP were held constant. Platinum nanocubes show the highest activity toward the conversion of 4-NP to 4-AP. The observed catalytic activity of the nanocubes is ascribed to its shape and higher surface-to-volume ratio property. In all, the shape of a nanoparticle plays a role in its catalytic activity. The catalytic performance of nanocubes compared to P-PtNPs is dependent on the reactivity of the cubic facets and the sharp edges.

https://doi.org/10.1021/acsomega.4c02948
ACS Omega 2024, 9, 38557−38568

3.10. Reusability and Regeneration of Shape-Dependent PtNPs Catalyst. To ensure a sustainable catalytic technology, the regeneration and reusability of the catalyst are vital requirements for practical environmental applications. For the catalyst recovery process, centrifugation was utilized to separate the PtNPs catalyst from 4-AP in solution after each degradation. PtNPs were then washed and dried overnight for the next catalytic degradation. Figure S6 shows a sustained and effective catalytic activity of four cycles. It is worth noting that the slight decrease in catalytic activity was due to the loss of catalyst during the purification process. Our promising results are in agreement with reports elsewhere.[42] In all, the PtNPs are potential catalysts for environmental remediation. The shape-dependent catalytic activity of anisotropic PtNPs has been compared to similar studies, as seen in Table 2. The conversion of 4-NP to 4-AP is dependent on the interplay of size and shape of the resultant nanoparticles. In our study, it can be concluded that when the size of the particles is constant, the shape of the particles influences the stability and catalytic performance of the catalyst.

3.11. Proposed Mechanism of PtNPs Catalytic Activity on the Reduction of 4-NP. The mechanism that explains the reduction of 4-nitrophenol in presence of PtNPs catalyst has been reported in several works. In this work, the catalytic activity of shape-dependent PtNPs on the reduction of 4-NP in wastewater obeys the Langmuir−Hinshelwood kinetic model.[41,46] To begin with, BH_{4-} ions are generated from $NaBH_4$ in water, the BH_4 ions act as a source of hydrogen ions that occupy the active site sites on the surface of the Pt particles forming H−Pt and $PtBH_3$ reaction intermediates. After this step, 4-NP molecules then adsorb on the surface of Pt-hydride, and PtNPs shuttle electrons to the nitro group of 4-NP from the BH_{4-} ion source.[42] The PtNPs hydride forms a complex with the 4-NP, reducing it to 4-AP. From this step, the 4-AP is detached from the surface of the catalyst and then recycled for the next catalytic phase, as seen in Figure S7. The high surface-to-volume ratio and reactivity of the multiple faces of the platinum nanocube enhance its catalytic activity for the degradation of 4-NP to 4-AP.

4. CONCLUSIONS

Monodispersed platinum nanocubes and nanopeanuts were synthesized at room temperature by reacting 4-QP and platinum ions in the molar ratio of 3:1 and 1:1, respectively. The 4-QP acted as the reducing and stabilizing agents. The hydroxyl and phosphate functional groups of 4′-QP were responsible for the rapid reduction of platinum ions and the growth of different shapes. The size and shape morphologies of PtNPs were determined and confirmed by UV−vis spectroscopy, XRD, TEM, and EDS analysis. The shape-dependent activity of P-PtNPs and C-PtNPs was investigated on both *C. freundii* and 4-NP in wastewater. The results demonstrated that the cubic shape of PtNPs enhances both antibacterial potency and catalytic performance. For instance, the catalytic conversion of 4-NP to 4-AP in the presence of C-PtNPs generated the highest conversion rate (k) = 0.0108 s^{-1}, while the k for the nanopeanuts catalyst was 0.00607 s^{-1}. Platinum Nanocubes exhibited higher catalytic activity due to the sharp edges of nanocube particles, and active facets of the nanocubes. Notably, parameters such as the concentration of PtNPs, particle sizes, and morphologies contribute to effective catalysis and antimicrobial activities. This work demonstrates that when the controlling factors of antimicrobial activity and catalysis are held constant, the resultant shape prevails and specifically enhances the nanoparticle performance. Future work will focus on the cytotoxicity effects of the shape-dependent PtNPs on MCF-7 breast cancer cells. This study shows the aqueous formulation of shaped−dependent platinum nanoparticles with superior performance. We envision that the 4′-QP would serve as a reliable reducing and stabilizing agent for the water-based synthesis of different anisotropic nanoparticles.

■ ASSOCIATED CONTENT

Supporting Information

The Supporting Information is available free of charge at https://pubs.acs.org/doi/10.1021/acsomega.4c02948.

In silico prediction of aqueous solubility of 4′-QP; minimum inhibitory concentration; results and discussion; aqueous solubility of 4′-QP; structure of Quercetin 4′-monophosphate (4′-QP); structures of quercetin; UV−vis of 4′-QP; computational analysis of water solubility and lipophilicity of QP and Quercetin; inhibition of *C. freundii* in the presence of an increasing concentration of P-PtNPs; MIC values of C-PtNPs (25 μg/mL) and P-PtNPs (45 μg/mL); reduction of 4-NP in wastewater using anisotropic platinum nanoparticles: wastewater sample preparation; and performance of anisotropic catalyst for the conversion of 4-NP to 4-AP; probable mechanism of catalytic activity of PtNPs on the conversion of 4-NP to 4-Ap in the presence of sodium borohydride (PDF)

■ AUTHOR INFORMATION

Corresponding Author

Omowunmi A. Sadik − *Department of Chemistry and Environmental Science BioSMART Center, New Jersey Institute of Technology, Newark, New Jersey 07102, United States;* orcid.org/0000-0001-8514-0608; Email: sadik@njit.edu

Authors

Gaddi B. Eshun − *Department of Chemistry and Environmental Science BioSMART Center, New Jersey Institute of Technology, Newark, New Jersey 07102, United States*

Francis J. Osonga − *Department of Chemistry and Environmental Science BioSMART Center, New Jersey Institute of Technology, Newark, New Jersey 07102, United States*

Complete contact information is available at: https://pubs.acs.org/10.1021/acsomega.4c02948

Notes

The authors declare no competing financial interest.

■ ACKNOWLEDGMENTS

The authors acknowledge the New Jersey Institute of Technology Start-up 172803 funds and the NJ Department of Environmental Protection Project #27K030).

■ REFERENCES

(1) Metri, B. C.; Jyothi, P.; Peerapur, B. V. Antibiotic resistance in Citrobacter spp. isolated from urinary tract infection. *Urol. Ann.* **2013**, *5* (4), 312.

(2) Oliveira, H.; Pinto, G.; Oliveira, A.; Oliveira, C.; Faustino, M. A.; Briers, Y.; Domingues, L.; Azeredo, J. Characterization and genome sequencing of a Citrobacter freundii phage CfP1 harboring a lysin active against multidrug-resistant isolates. *Appl. Microbiol. Biotechnol.* **2016**, *100* (24), 10543−10553.
(3) Poirel, L.; Ros, A.; Carricajo, A.; Berthelot, P.; Pozzetto, B.; Bernabeu, S.; Nordmann, P. Extremely drug-resistant Citrobacter freundii isolate producing NDM-1 and other carbapenemases identified in a patient returning from India. *Antimicrob. Agents Chemother.* **2011**, *55* (1), 447−448.
(4) Brackett, C. M.; Melander, R. J.; An, I. H.; Krishnamurthy, A.; Thompson, R. J.; Cavanagh, J.; Melander, C. Small-Molecule Suppression of β-Lactam Resistance in Multidrug-Resistant Gram-Negative Pathogens. *J. Med. Chem.* **2014**, *57* (17), 7450−7458.
(5) Chen, S.; Yu, Z.; Wang, Y.; Tang, J.; Zeng, Y.; Liu, X.; Tang, D. Block-polymer-restricted sub-nanometer Pt nanoclusters nanozyme-enhanced immunoassay for monitoring of cardiac troponin I. *Anal. Chem.* **2023**, *95* (38), 14494−14501.
(6) Zeng, R.; Li, Y.; Hu, X.; Wang, W.; Li, Y.; Gong, H.; Xu, J.; Huang, L.; Lu, L.; Zhang, Y.; et al. Atomically site synergistic effects of dual-atom nanozyme enhances peroxidase-like properties. *Nano Lett.* **2023**, *23* (13), 6073−6080.
(7) Osonga, F. J.; Akgul, A.; Yazgan, I.; Akgul, A.; Ontman, R.; Kariuki, V. M.; Eshun, G. B.; Sadik, O. A. Flavonoid-derived anisotropic silver nanoparticles inhibit growth and change the expression of virulence genes in Escherichia coli SM10. *RSC Adv.* **2018**, *8* (9), 4649−4661.
(8) Osonga, F. J.; Le, P.; Luther, D.; Sakhaee, L.; Sadik, O. A. Water-based synthesis of gold and silver nanoparticles with cuboidal and spherical shapes using luteolin tetraphosphate at room temperature. *Environ. Sci.: Nano* **2018**, *5* (4), 917−932.
(9) Osonga, F. J.; Eshun, G.; Kalra, S.; Yazgan, I.; Sakhaee, L.; Ontman, R.; Jiang, S.; Sadik, O. A. Influence of Particle Size and Shapes on the Antifungal Activities of Greener Nanostructured Copper against Penicillium italicum. *ACS Agric. Sci. Technol.* **2022**, *2*, 42−56.
(10) Yaqoob, A. A.; Umar, K.; Ibrahim, M. N. M. Silver nanoparticles: various methods of synthesis, size affecting factors and their potential applications−a review. *Appl. Nanosci.* **2020**, *10* (5), 1369−1378.
(11) Eshun, G. B.; Osonga, F. J.; Erdogan, T.; Gölcü, A.; Sadik, O. A. Controlled synthesis and computational analysis of gold nanostars for the treatment of Fusarium oxysporum. *RSC Adv.* **2023**, *13* (31), 21781−21792.
(12) Lin, X.; Wang, J.; Han, X.; Wu, M.; Kuga, S.; Huang, Y. Use of Lignin and Hemicelluloses for Facial Synthesis of Gold, Platinum, and Palladium Nanoparticles. *J. Bioresour. Bioprod.* **2017**, *2*, 149−152.
(13) Pandey, S.; Mishra, S. B. Catalytic reduction of p-nitrophenol by using platinum nanoparticles stabilised by guar gum. *Carbohydr. Polym.* **2014**, *113*, 525−531.
(14) Kariuki, V. M.; Zhang, J.; Parlinska, M.; Sadik, O. A. 3D π-conjugated poly (amic) acid polymer as support matrices for ethanol electro-oxidation on palladium and platinum catalysts. *Electrocatalysis* **2016**, *7*, 317−325.
(15) Kariuki, V. M.; Yazgan, I.; Akgul, A.; Kowal, A.; Parlinska, M.; Sadik, O. A. Synthesis and catalytic, antimicrobial and cytotoxicity evaluation of gold and silver nanoparticles using biodegradable, Π-conjugated polyamic acid. *Environ. Sci.: Nano* **2015**, *2* (5), 518−527.
(16) Osonga, F. J.; Onyango, J. O.; Mwilu, S. K.; Noah, N. M.; Schulte, J.; An, M.; Sadik, O. A. Synthesis and characterization of novel flavonoid derivatives via sequential phosphorylation of quercetin. *Tetrahedron Lett.* **2017**, *58* (15), 1474−1479.
(17) Kiehlbauch, J. A.; Hannett, G. E.; Salfinger, M.; Archinal, W.; Monserrat, C.; Carlyn, C. Use of the National Committee for Clinical Laboratory Standards guidelines for disk diffusion susceptibility testing in New York state laboratories. *J. Clin. Microbiol.* **2000**, *38* (9), 3341−3348.
(18) Espinel-Ingroff, A.; Fothergill, A.; Peter, J.; Rinaldi, M.; Walsh, T. Testing conditions for determination of minimum fungicidal concentrations of new and established antifungal agents for Aspergillus spp.: NCCLS collaborative study. *J. Clin. Microbiol.* **2002**, *40* (9), 3204−3208.
(19) Vukoja, D.; Vlainić, J.; Ljolić Bilić, V.; Martinaga, L.; Rezić, I.; Brlek Gorski, D.; Kosalec, I. Innovative Insights into In vitro activity of colloidal platinum nanoparticles against ESBL-Producing Strains of Escherichia coli and Klebsiella pneumoniae. *Pharmaceutics* **2022**, *14* (8), 1714.
(20) Charannya, S.; Duraivel, D.; Padminee, K.; Poorni, S.; Nishanthine, C.; Srinivasan, M. R. Comparative evaluation of antimicrobial efficacy of silver nanoparticles and 2% chlorhexidine gluconate when used alone and in combination assessed using agar diffusion method: an in vitro study. *Contemp. Clin. Dent.* **2018**, *9* (6), S204.
(21) Zhou, A.; Kikandi, S.; Sadik, O. A. Electrochemical degradation of quercetin: Isolation and structural elucidation of the degradation products. *Electrochem. Commun.* **2007**, *9* (9), 2246−2255.
(22) Corrente, G. A.; Malacaria, L.; Beneduci, A.; Furia, E.; Marino, T.; Mazzone, G. Experimental and theoretical study on the coordination properties of quercetin towards aluminum (III), iron (III) and copper (II) in aqueous solution. *J. Mol. Liq.* **2021**, *325*, 115171.
(23) Dauthal, P.; Mukhopadhyay, M. Biofabrication, characterization, and possible bio-reduction mechanism of platinum nanoparticles mediated by agro-industrial waste and their catalytic activity. *J. Ind. Eng. Chem.* **2015**, *22*, 185−191.
(24) Zheng, B.; Kong, T.; Jing, X.; Odoom-Wubah, T.; Li, X.; Sun, D.; Lu, F.; Zheng, Y.; Huang, J.; Li, Q. Plant-mediated synthesis of platinum nanoparticles and its bioreductive mechanism. *J. Colloid Interface Sci.* **2013**, *396*, 138−145.
(25) Liu, H.; Zhang, H.; Wang, J.; Wei, J. Effect of temperature on the size of biosynthesized silver nanoparticle: deep insight into microscopic kinetics analysis. *Arab. J. Chem.* **2020**, *13* (1), 1011−1019.
(26) Demortiere, A.; Launois, P.; Goubet, N.; Albouy, P.-A.; Petit, C. Shape-controlled platinum nanocubes and their assembly into two-dimensional and three-dimensional superlattices. *J. Phys. Chem. B* **2008**, *112* (46), 14583−14592.
(27) Zhang, X.; Xia, Z.; Huang, Y.; Jia, Y.; Sun, X.; Li, Y.; Li, X.; Wu, R.; Liu, A.; Qi, X.; et al. Shape-controlled synthesis of Pt nanopeanuts. *Sci. Rep.* **2016**, *6* (1), 31404.
(28) Ren, J.; Tilley, R. D. Preparation, self-assembly, and mechanistic study of highly monodispersed nanocubes. *J. Am. Chem. Soc.* **2007**, *129* (11), 3287−3291.
(29) Venu, R.; Ramulu, T.; Anandakumar, S.; Rani, V.; Kim, C. Bio-directed synthesis of platinum nanoparticles using aqueous honey solutions and their catalytic applications. *Colloids Surf., A* **2011**, *384* (1−3), 733−738.
(30) Agrawal, N.; Mishra, P.; Ranjan, R.; Awasthi, P.; Srivastava, A.; Prasad, D.; Kohli, E. Nano-cubes over nano-spheres: shape dependent study of silver nanomaterial for biological applications. *Bull. Mater. Sci.* **2021**, *44* (3), 191.
(31) Ren, J.; Wang, W.; Sun, S.; Zhang, L.; Wang, L.; Chang, J. Crystallography facet-dependent antibacterial activity: the case of Cu2O. *Ind. Eng. Chem. Res.* **2011**, *50* (17), 10366−10369.
(32) Pal, S.; Tak, Y. K.; Song, J. M. Does the antibacterial activity of silver nanoparticles depend on the shape of the nanoparticle? A study of the gram-negative bacterium Escherichia coli. *Appl. Environ. Microbiol.* **2007**, *73* (6), 1712−1720.
(33) Gupta, K.; Chundawat, T. S. Bio-inspired synthesis of platinum nanoparticles from fungus Fusarium oxysporum: its characteristics, potential antimicrobial, antioxidant and photocatalytic activities. *Mater. Res. Express* **2019**, *6* (10), 1050d6.
(34) Aygun, A.; Gülbagca, F.; Ozer, L. Y.; Ustaoglu, B.; Altunoglu, Y. C.; Baloglu, M. C.; Atalar, M. N.; Alma, M. H.; Sen, F. Biogenic platinum nanoparticles using black cumin seed and their potential usage as antimicrobial and anticancer agent. *J. Pharm. Biomed. Anal.* **2020**, *179*, 112961.

https://doi.org/10.1021/acsomega.4c02948
ACS Omega 2024, 9, 38557−38568

(35) Kameya, Y.; Hayashi, T.; Motosuke, M. Stability of platinum nanoparticles supported on surface-treated carbon black. *Appl. Catal., B* **2016**, *189*, 219−225.
(36) Tenea, G. N.; Angamarca, E.; Olmedo, D. Combinations of Peptide-Protein Extracts from Native Probiotics Suppress the Growth of Multidrug-Resistant Staphylococcus aureus and Citrobacter freundii via Membrane Perturbation and Ultrastructural Changes. *Antibiotics* **2022**, *11* (2), 154.
(37) Ruiz, A. L.; Garcia, C. B.; Gallón, S. N.; Webster, T. J. Novel silver-platinum nanoparticles for anticancer and antimicrobial applications. *Int. J. Nanomed.* **2020**, *15*, 169−179.
(38) Kankala, R. K.; Liu, C.-G.; Yang, D.-Y.; Wang, S.-B.; Chen, A.-Z. Ultrasmall platinum nanoparticles enable deep tumor penetration and synergistic therapeutic abilities through free radical species-assisted catalysis to combat cancer multidrug resistance. *Chem. Eng. J.* **2020**, *383*, 123138.
(39) Dharmaraja, A. T. Role of reactive oxygen species (ROS) in therapeutics and drug resistance in cancer and bacteria. *J. Med. Chem.* **2017**, *60* (8), 3221−3240.
(40) Shoshan, M. S.; Vonderach, T.; Hattendorf, B.; Wennemers, H. Peptide-coated platinum nanoparticles with selective toxicity against liver cancer cells. *Angew. Chem., Int. Ed.* **2019**, *58* (15), 4901−4905.
(41) Nguyen, V. P.; Le Trung, H.; Nguyen, T. H.; Hoang, D.; Tran, T. H. Advancement of microwave-assisted biosynthesis for preparing Au nanoparticles using Ganoderma lucidum extract and evaluation of their catalytic reduction of 4-nitrophenol. *ACS Omega* **2021**, *6* (47), 32198−32207.
(42) Sundarapandi, M.; Viswanathan, P.; Sivakumar, S.; Ramaraj, R. Catalytic activities of mono-and bimetallic (Gold/Silver) nanoshell-coated gold nanocubes toward catalytic reduction of nitroaromatics. *Langmuir* **2018**, *34* (46), 13897−13904.
(43) Dang-Bao, T.; Nguyen, L.-N.; Lam, H.-H. Corncob-derived nanocellulose-supported palladium nanoparticles towards catalytic reduction of 4-nitrophenol. In *Materials Today: Proceedings*; Elsevier, 2023.
(44) Khoshnamvand, M.; Huo, C.; Liu, J. Silver nanoparticles synthesized using Allium ampeloprasum L. leaf extract: characterization and performance in catalytic reduction of 4-nitrophenol and antioxidant activity. *J. Mol. Struct.* **2019**, *1175*, 90−96.
(45) Yuan, C.-G.; Huo, C.; Gui, B.; Liu, P.; Zhang, C. Green synthesis of silver nanoparticles using Chenopodium aristatum L. stem extract and their catalytic/antibacterial activities. *J. Cluster Sci.* **2017**, *28*, 1319−1333.
(46) Noh, J.-H.; Meijboom, R. Catalytic evaluation of dendrimer-templated Pd nanoparticles in the reduction of 4-nitrophenol using Langmuir−Hinshelwood kinetics. *Appl. Surf. Sci.* **2014**, *320*, 400−413.

https://doi.org/10.1021/acsomega.4c02948
ACS Omega 2024, 9, 38557−38568